Charge-Ordering in Manganates

C. N. R. Rao,*[,†,‡] Anthony Arulraj,[†] P. N. Santosh,[†] and A. K. Cheetham[‡]

CSIR Centre of Excellence in Chemistry & Solid State and Structural Chemistry Unit, Indian Institute of Science, Bangalore 560012, India, and Materials Research Laboratory, University of California, Santa Barbara, California 93106

Received April 30, 1998. Revised Manuscript Received June 11, 1998

Ordering of Mn^{3+} and Mn^{4+} ions occurs in the rare earth manganates of the general composition $Ln_{1-x}A_xMnO_3$ (Ln = rare earth, A = Ca, Sr). Such charge-ordering is associated with antiferromagnetic and insulating properties. This phenomenon is to be contrasted with the ferromagnetic metallic behavior that occurs when double-exchange between the Mn^{3+} and Mn^{4+} ions predominates. Two distinct types of charge-ordering can be delineated. In one, a ferromagnetic metallic (FMM) state transforms to the charge-ordered (CO) state on cooling. In the other scenario, the CO state is found in the paramagnetic ground state and there is no ferromagnetism down to the lowest temperatures. Magnetic fields transform the CO state to the FMM state, when the average radius of the A-site cations is sufficiently large ($\langle r_A \rangle > 1.17$ Å). Chemical melting of the CO state by Cr^{3+} substitution in the Mn site is also found only when $\langle r_A \rangle \gtrsim 1.17$ Å. The effect of the size of the A-cations on the Mn−O−Mn angle is not enough to explain the observed variations of the charge-ordering temperature as well as the ferromagnetic Curie temperature T_c. An explanation based on a competition between the Mn and A-cation orbitals for σ-bonding with the oxygen ρ_σ orbitals is considered to account for the large changes in T_c and hence the true bandwidth, with $\langle r_A \rangle$. Effects of radiation, electric field, and other factors on the CO state are discussed along with charge-ordering in other manganate systems. Complex phase transitions, accompanied by changes in electronic and magnetic properties, occur in manganates with critical values of $\langle r_A \rangle$ or bandwidth. Charge-ordering is found in layered manganates, $Bi_xCa_{1-x}MnO_3$ and $CaMnO_{3-\delta}$.

Contents

1. Introduction

Charge-ordering refers to the ordering of the metal ions in different oxidation states in specific lattice sites of a mixed valent material. Such ordering generally localizes the electrons in the material, rendering it insulating or semiconducting because when the charges are localized, electrons cannot readily hop from one cation site to another. Charge-ordering is not a new phenomenon in metal oxides. One of the earliest examples of charge-ordering in inorganic solids is that of Fe_3O_4 (magnetite), which undergoes a disorder−order transition, popularly known as the Verwey transition, at 120 K. The literature abounds in studies of this transition, and the topic continues to attract attention.[1] The Verwey transition in Fe_3O_4, which occurs well below the ferrimagnetic transition at 860 K, is very sensitive to oxygen stoichiometry and cation substitutions. The low-temperature ordered state in Fe_3O_4 is complex, giving rise to a low crystal symmetry (monoclinic or triclinic) and involving the distribution of Fe^{3+} and Fe^{2+} over several sites.[2,3] Complex charge-ordering is also found in the perovskite, $La_{1-x}Sr_xFeO_3$,[4] and quasi-two-dimensional $La_{2-x}Sr_xNiO_4$.[5] The charge-ordering transition in $La_{1.67}Sr_{0.33}NiO_4$ occurs around 240 K, accompanied by a structural change and opening up of a gap.[5] Charge-ordering in rare earth manganates of the general formula, $Ln_{1-x}A_xMnO_3$ (Ln = rare earth, A = alkaline earth) is particularly fascinating, being associated with novel properties that are sensitive to electronic and geometric factors. The study of charge-ordering in these manganates has recently received much attention because of the colossal magnetoresistance (CMR) exhibited by these materials, although charge-ordering itself had been noticed by Wollan Kochler in 1955 and later by Jirak et al. in 1985.[6,7]

Rare earth manganates of the general formula $Ln_{1-x}A_xMnO_3$ ($x \approx 0.3$) become ferromagnetic due to the double-exchange interaction involving Mn^{3+}−O−Mn^{4+} units. Around the ferromagnetic Curie temperature, T_c, the materials also undergo an insulator−metal transi-

* Corresponding author.
† Indian Institute of Science.
‡ University of California, Santa Barbara.

10.1021/cm980318e CCC: $15.00
Published on Web 10/02/1998

tion. Metallicity below T_c occurs because only those electrons that have ferromagnetically aligned spins are involved in the conduction process. When magnetic fields are applied to these materials, the resistivity decreases greatly, particularly in the region of the T_c or the insulator−metal transition. The decrease in resistivity can be almost 100% and, hence, the use of the term colossal while referring to the magnetoresistance in these materials. The ferromagnetic T_c in the manganates increases with pressure or with the average size of the A-site cations. Jahn−Teller distortion due to Mn^{3+} ions is prominent in the insulating regime.

Charge-ordering of the Mn^{3+} and Mn^{4+} ions in the rare earth manganates favors antiferromagnetism and insulating behavior. Charge-ordering competes with double-exchange, giving rise to an unusual range of properties that are sensitive to factors such as the size of the A-site cations. The cooperative Jahn−Teller effect induces additional effects such as lattice distortion and electron localization in the charge-ordered (CO) state. In this article, we shall discuss the various features and phenomena associated with charge-ordering in rare earth manganates, with particular emphasis on recent findings related to the factors affecting the phenomenon. Some of the factors discussed deal with the melting of the CO state to a ferromagnetic metallic state by chemical substitution or by the application of magnetic fields, external or internal pressure, electric field, and laser radiation. We shall also briefly examine the evidence for charge-ordering in some related manganese oxides.

2. Typical Scenarios

Charge-ordering in the manganates, $Ln_{1-x}A_xMnO_3$, is found in the compositions $0.30 \leq x \leq 0.75$. To understand the gross features of the charge-ordering phenomenon in these materials, we shall first examine the properties of a few typical members such as $Nd_{0.5}Sr_{0.5}MnO_3$ and $Pr_{1-x}Ca_xMnO_3$ ($0.3 \leq x \leq 0.5$). $Nd_{0.5}Sr_{0.5}MnO_3$ is a ferromagnetic metal (FMM) with a T_c of 250 K. On cooling, the FMM state transforms to a CO antiferromagnetic (CE type) state at ∼150 K ($T_{CO} = T_N$).[8] At T_{CO}, we notice a change in lattice parameters and a sharp rise in resistivity (Figure 1). The space group changes from *Imma* to *Pnmm* (or $Pnm2_1$) at T_{CO}.[9] Scanning tunneling spectroscopy under vacuum has shown that a charge-ordering gap of ∼0.3 eV develops across T_{CO} (Figure 2).[10] Application of magnetic fields transforms the CO state to the FMM state and the transition is first order, as evidenced from the hesteretic behavior shown in Figure 3. Unlike $Nd_{0.5}Sr_{0.5}MnO_3$, $Pr_{0.5}Sr_{0.5}MnO_3$ does not show evidence for charge-ordering at low temperatures; instead, it undergoes a transition from a FMM state to an insulating antiferromagnetic (AFM) state (A-type) at 140 K.[11]

$Pr_{1-x}Ca_xMnO_3$ ($0.3 \leq x \leq 0.5$) has a paramagnetic insulating ground state around room temperature and gets charge-ordered on cooling.[12] When $x = 0.35$, T_{CO} is ∼240 K and T_N occurs at even lower temperatures (∼140 K). The insulating CO state can be melted to a FMM state on the application of high magnetic fields (Figure 4). $Pr_{1-x}Ca_xMnO_3$ compositions do not show ferromagnetism on their own, at any temperature. A similar behavior is also obtained in $Nd_{0.5}Ca_{0.5}MnO_3$.[13]

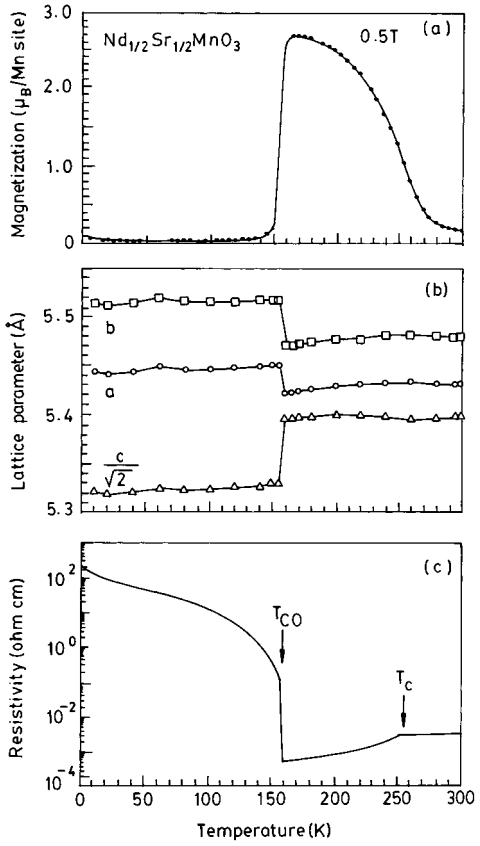

Figure 1. Temperature variation of (a) magnetization, (b) lattice parameters, and (c) resistivity of $Nd_{0.5}Sr_{0.5}MnO_3$ (from Kuwahara et al.[8]).

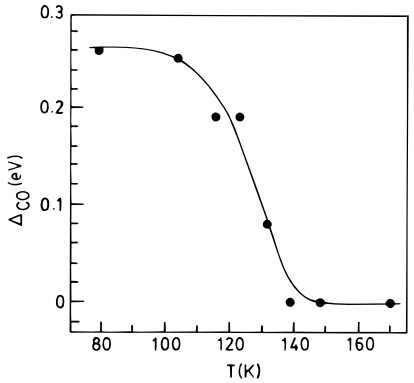

Figure 2. Temperature dependence of the charge-ordering gap, Δ_{CO}, in $Nd_{0.5}Sr_{0.5}MnO_3$ (from Biswas et al.[10]).

Application of magnetic fields enforces a ferromagnetic spin alignment in these materials and drives them to a metallic state by the double-exchange mechanism,[14] as in the rare earth manganates exhibiting CMR.[7] In Figure 5, we show the temperature−magnetic field (T−H) phase diagrams of $Nd_{0.5}Sr_{0.5}MnO_3$ and $Pr_{0.65}Ca_{0.35}MnO_3$ to illustrate the slight significant differences between the two systems.[15] It should be noted that in the CO state of $Nd_{0.5}Ca_{0.5}MnO_3$ and such materials, Mn^{3+} and Mn^{4+} occur alternately, accompanied by a zigzag arrangement of long and short Mn−O distances.[13] The CO state in $Nd_{0.5}Ca_{0.5}MnO_3$ has been found to be destroyed on application of a 6 T magnetic field.[13] It was recently found that the magnetic field effect on this solid is very sensitive to stoichiometry.[12b] Thus, stoichiometric $Nd_{0.5}Ca_{0.5}MnO_3$ seems to show

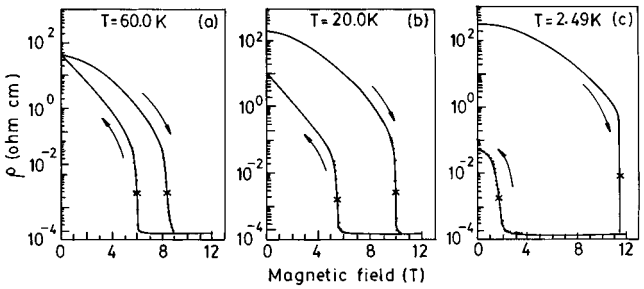

Figure 3. Changes in the resistivity of $Nd_{0.5}Sr_{0.5}MnO_3$ with increasing and decreasing fields. Notice the sharp jump in resistivity at the lower and upper critical fields (from Kuwahara et al.[8]).

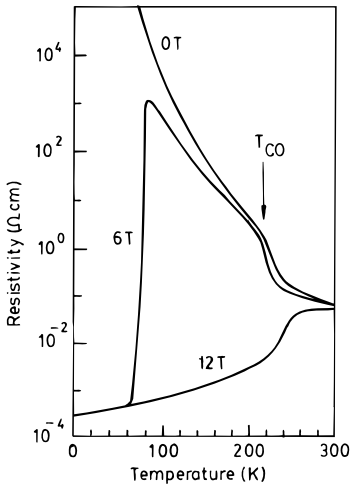

Figure 4. Temperature variation of resistivity of $Pr_{0.65}Ca_{0.35}MnO_3$ in the absence and presence of magnetic fields (from Tomioka et al.[12]).

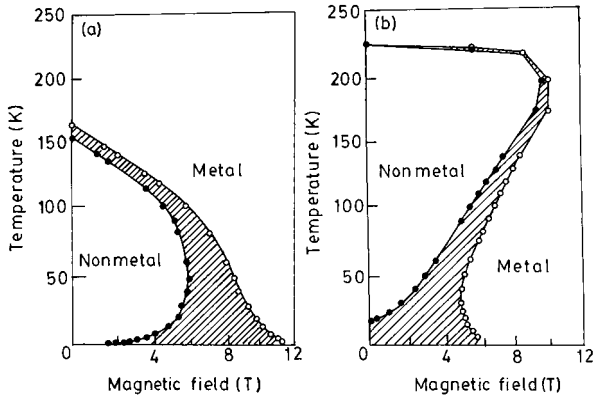

Figure 5. Electronic phase diagrams of (a) $Nd_{0.5}Sr_{0.5}MnO_3$ and (b) $Pr_{0.65}Ca_{0.35}MnO_3$ (from Tokura et al.[15]). Hatched region shows the hesteretic regime.

melting of the CO state only when a high magnetic field (>10 T) is applied. The melting of the CO state in $Pr_{0.5}Ca_{0.5}MnO_3$ occurs at a lower field. We have verified these observations as well. The destruction of the CO state is accompanied by the appearance of an FMM state and a structural transition.[12b] The stability of the CO state is related to the collinear AFM ordering of the Mn moments.

In $La_{0.35}Ca_{0.65}MnO_3$ charge-ordering is observed at 260 K, accompanied by an increase in the sound velocity and anomalies in the heat capacity and the activation energy for conduction.[16] The CO state occurs in the paramagnetic regime and T_N is found at a much lower temperature (~160 K). There is a large anisotropic lattice distortion and a distortion of the MnO_6 octahedra on charge-ordering. $La_{0.5}Ca_{0.5}MnO_3$ shows ferromagnetic and antiferromagnetic (charge-ordering) transitions at 225 and 170 K, respectively.[17] Between T_c and T_N, unusual variations in the X-ray diffraction profiles are observed, suggesting the possible occurrence of a continuous distribution of lattice parameters or of a number of discrete phases with a coherence length larger than the intrinsic coherence length for X-rays. Jahn−Teller distortion develops in this temperature region, with the d_{z^2} orbitals oriented perpendicular to the orthorhombic *b*-axis. Magnetic domain boundaries break the coherence of a spin ordering of the Mn^{3+} sites while preserving the coherence of a spin ordering on the Mn^{4+} sublattice, as well as the identity of the two sublattices. The resemblance between these structures and the structural charge-ordering and discommensuration domain boundaries, observed by electron diffraction and lattice imaging, suggests that long-range charge-ordering coexists with quasicommensurate orbital ordering. Static charge stripes characterize the insulating antiferromagnetic ground state of $La_{1-x}Ca_xMnO_3$ ($x > 0.5$), somewhat similar to the stripe phases found in high T_c cuprates.[18] Extremely stable pairs of $Mn^{3+}O_6$ stripes associated with large lattice contractions [due to Jahn−Teller (J−T) effect] separated by undistorted $Mn^{4+}O_6$ octahedra are found in these $La_{1-x}Ca_xMnO_3$ compositions.[19] These periodicities adopt integer values between two and five times the lattice parameter of the orthorhombic unit cell, corresponding to the commensurate carrier concentrations $x = 1/2$, 2/3, 3/4, and 4/5. For other values of x, the charge-ordering pattern is a mixture of two adjacent commensurate configurations. These J−T stripes seem to build blocks of the CO state in the manganese oxides.

The melting or the destruction of the CO state by magnetic fields was characteristic of the various manganates discussed hitherto. However, magnetic fields have no effect on the insulating CO states in manganates where the average radius (Shannon value for 9-fold coordination) of the A-site cations, $\langle r_A \rangle$, is small. Thus, $Y_{0.5}Ca_{0.5}MnO_3$ ($\langle r_A \rangle = 1.13$ Å) remains a CO insulator even on the application of high magnetic fields.[20] It appears that all the $Ln_{0.5}Ca_{0.5}MnO_3$ compositions with $\langle r_A \rangle < 1.17$ Å show this behavior (Figure 6). We see from the figure that only in $Nd_{0.5}Ca_{0.5}MnO_3$ ($\langle r_A \rangle = 1.17$ Å) does the CO state transform to a metal-like state under a magnetic field of 6 T. We therefore have a situation wherein different types of CO states can be delineated based on the effect of magnetic fields. We show this aspect schematically in Figure 7 and list some relevant data in Table 1. The manganates in the $\langle r_A \rangle$ regime with robust CO states are clearly dominated by cooperative J−T effect and related lattice distortions. In fact, the lattice distortion index in these manganates increases with decreasing $\langle r_A \rangle$, reaching a value of 1.8% in $Y_{0.5}Ca_{0.5}MnO_3$.

3. Effect of the Size of the A-Site Cations

In Figure 8, we show a schematic diagram to describe the different types of behavior of the manganates depending on $\langle r_A \rangle$. The region D corresponds to the manganates where magnetic fields have no effect on the

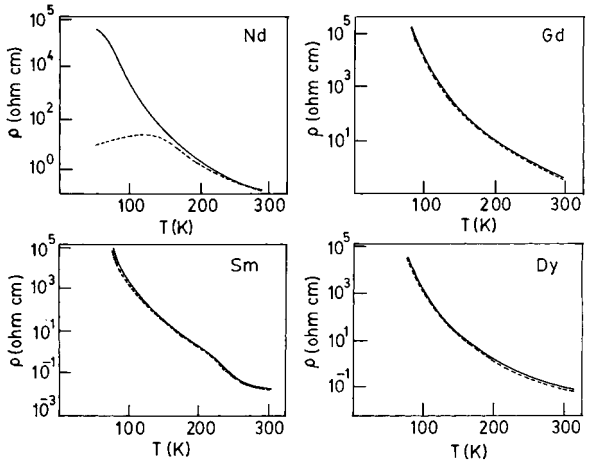

Figure 6. Electrical resistivity of $Ln_{0.5}Ca_{0.5}MnO_3$ in the absence (full curve) and presence (broken curve) of a magnetic field of 6 T (from Arulraj et al.[20b]). The data on $Nd_{0.5}Ca_{0.5}MnO_3$ are from an older sample. When the stoichiometry is exact, higher magnetic fields seem to be necessary to melt the CO state.

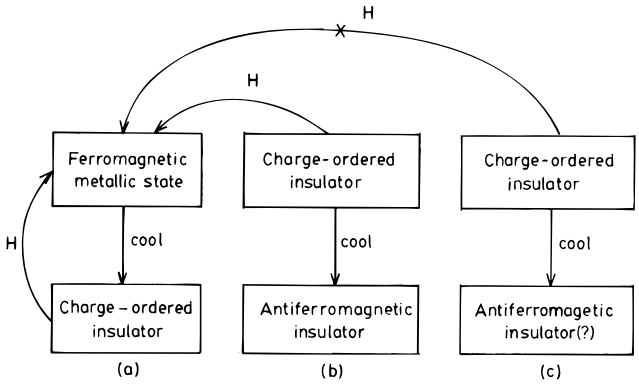

Figure 7. Different types of CO states in rare earth manganates as delineated by the effect of magnetic fields. The $\langle r_A \rangle$ value decreases from left to right. Scenarios (a), (b), and (c) correspond to $Nd_{0.5}Sr_{0.5}MnO_3$ ($\langle r_A \rangle = 1.24$ Å), $Nd_{0.5}Ca_{0.5}MnO_3$ ($\langle r_A \rangle = 1.17$ Å), and $Y_{0.5}Ca_{0.5}MnO_3$ ($\langle r_A \rangle = 1.13$ Å), respectively.

Table 1. Stable (Near Room Temperature) Phases, $\langle r_A \rangle$ Values, and Charge-Ordering Temperatures, T_{CO}, in $Ln_{0.5}A_{0.5}MnO_3$

	A = Ca			A = Sr		
Ln	$\langle r_A \rangle$, Å	stable phase	T_{CO} (K)	$\langle r_A \rangle$, Å	stable phase	T_{CO} (K)
Y	1.127	CO[a]	260			
Dy	1.132	CO[a]	260			
Gd	1.143	CO[a]	260	1.208	spin glass	
Nd	1.172	CO[b]	240	1.236	FMM[d]	150
Pr	1.179	CO[b]	240	1.244	FMM[d]	(140)[e]
La	1.198	PMI[c]	170	1.263	FMM[d]	0

[a] Magnetic field (6 T) has no effect. [b] Magnetic field (6 T) melts the CO state to a FMM state. [c] T_c value is 225 K. [d] T_c values are 250, 260, and 360 K, respectively, in Nd, Pr, and La systems. [e] T_N value; no CO transition is found.

insulating CO state (e.g., $Y_{0.5}Ca_{0.5}MnO_3$). Region B corresponds to manganates with a FMM ground state, such as $Nd_{0.5}Sr_{0.5}MnO_3$ ($\langle r_A \rangle = 1.24$ Å). Region A involves manganates showing CMR, with the FMM state occurring on cooling the paramagnetic insulating state. Magnetic fields affect the CO states in the $\langle r_A \rangle$ regime 1.17−1.24 Å. The occurrence of two types of CO states can be understood qualitatively in terms of the variation of the exchange couplings (J_{FM} and J_{AFM}) and

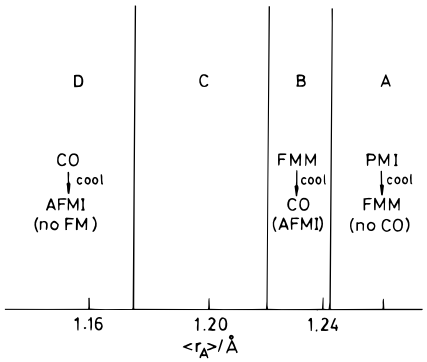

Figure 8. Schematic diagram showing different charge-ordering behaviors of $Ln_{0.5}A_{0.5}MnO_3$ depending on $\langle r_A \rangle$. Key: FMM, ferromagnetic metal; PMI, paramagnetic insulator; AFMI, antiferromagnetic insulator; CO, charge-ordered state.

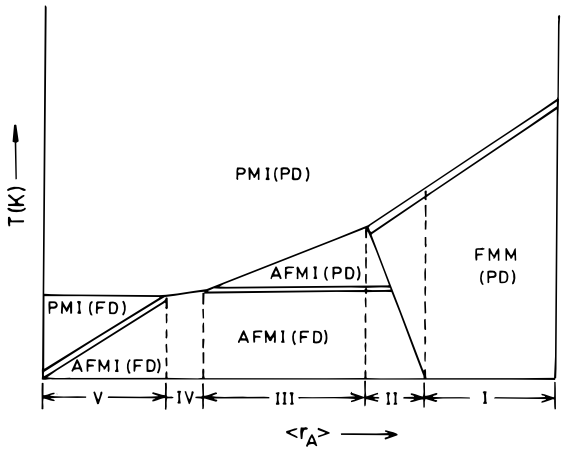

Figure 9. Schematic phase diagram of $Ln_{0.5}A_{0.5}MnO_3$. Double line represents a second-order transition and a single line represents a first-order transition. Key: PD, paradistortive; FD, ferrodistortive (from Kumar and Rao[21]).

the J−T energy (E_{JT}) with $\langle r_A \rangle$. Although J_{FM} and J_{AFM} are expected to decrease with a decrease in $\langle r_A \rangle$, E_{JT} would be insensitive to $\langle r_A \rangle$. In the small $\langle r_A \rangle$ regime, the cooperative J−T effect involving long-range elastic strain would dominate charge-ordering. At moderate values of $\langle r_A \rangle$, when $J_{AFM} > E_{JT}$, J_{FM}, the e_g electrons that are localized magnetically lower the configuration energy by charge-ordering (e.g., $Nd_{0.5}Sr_{0.5}MnO_3$). Such a CO state would be sensitive to magnetic fields. The gain in Zeeman energy resulting from the application of a magnetic field stabilizes the FMM state over the antiferromagnetic insulating state. In the small $\langle r_A \rangle$ regime, the manganates could be considered to have pseudo-spins (representing the single ion J−T effect) that do not couple to the magnetic field.

A general phase diagram for a fixed composition of the manganates ($Ln_{0.5}A_{0.5}MnO_3$) in the temperature (T) − $\langle r_A \rangle$ plane has been constructed by Kumar and Rao[21] based on the manner in which J_{FM} and J_{AFM} vary with $\langle r_A \rangle$. The ferromagnetic T_c in the manganates decreases more markedly with $\langle r_A \rangle$ than the T_N values in the managanates, suggesting that J_{AFM} decreases more markedly than J_{FM}. Based on these considerations, the qualitative phase diagram in Figure 9 can be drawn. We notice that the highest temperature phase is always a paramagnetic insulator (PMI), which is paradistortive (PD). The insulating behavior results from the single-ion J−T distortion as well as the blocking of hopping

by strong Hund coupling to the paramagnetically disordered Mn spins.

An examination of the different regions of the phase diagram in Figure 9 is revealing. In region I, we have the PMI−FMM transition on cooling, as in many of the manganates exhibiting giant magnetoresistance; this region corresponds to region A of Figure 8. In region II, $J_{AFM} > J_{FM}$, but the extra entropy of the itinerant carriers in the FM state favors the metallic phase. At low temperatures, however, one may expect a first-order FMM−AFMI transition, the latent heat per Mn^{3+} being $\sim k_B T \ln 2$. Region II of Figure 9 corresponds to region B of Figure 8 and is exemplified by $Nd_{0.5}Sr_{0.5}MnO_3$. In region III, J_{AFM} dominates and a first-order PMI−AFMI transition can occur; at low temperatures, charge-ordering would be expected. Complex magnetic properties can be found in regions III and IV (corresponding to region C in Figure 8) arising from the coupling with other parameters (e.g., ferroelastic). Region V is expected to be dominated by J−T effect, wherein the pseudo-spin state undergoes a first-order transition (due to loss of communal entropy) on cooling to a FD-insulating phase. Region V corresponds to region D in Figure 8 and is exemplified by $Y_{0.5}Ca_{0.5}MnO_3$. Charge-ordering in Region V is distinctly different from that in region II, as is indeed observed experimentally.

The two types of charge-ordering already discussed are different from the charge density wave (CDW)-type ordering caused by Fermi-surface nesting. These are more like the infinitely adaptive structures and would occur over a continuous range of doping. Such lattice effects have been found in $Nd_{0.25}La_{0.25}Ca_{0.5}MnO_3$, as discussed later in section 7. If one considers the blocking of the delocalization of e_g electrons by AFM or J−T effects as an enhancement of the effective carrier mass, the CO state may indeed be viewed as Wigner crystallization at low temperatures, even for high carrier concentrations. The complexity of region C will be discussed later in section 7, with some examples.

Why does $\langle r_A \rangle$ affect the nature of the CO state as well as the T_c in the ferromagnetic state so markedly? It is known that $\langle r_A \rangle$ directly determines the Mn−O−Mn angle and the average Mn−O distance in the manganates. In Figure 10, we have plotted the known values of the Mn−O−Mn angle and the average Mn−O distance in $Ln_{0.7}A_{0.3}MnO_3$[22] and $Ln_{0.5}A_{0.5}MnO_3$[20b,23] against $\langle r_A \rangle$. The Mn−O−Mn angle increases smoothly with $\langle r_A \rangle$, nearly independent of the composition, giving a common curve for both the $Ln_{0.5}A_{0.5}MnO_3$ and $Ln_{0.7}A_{0.3}MnO_3$ systems. The plot of the average Mn−O distance (d_{Mn-O}) against $\langle r_A \rangle$, however, shows a minimum at 1.24 Å in $Ln_{0.7}A_{0.3}MnO_3$.[22] The minimum is a geometrical necessity and is readily understood. In $Ln_{0.5}A_{0.5}MnO_3$, the Mn−O distance become nearly constant when $\langle r_A \rangle > 1.24$ Å. We can estimate the apparent one-electron bandwidth, W_a, of the manganates by using the following relation[24]

$$W_a \propto \cos \omega / d_{Mn-O}^{3.5} \qquad (1)$$

where $\omega = {}^1/_2(\pi - \langle Mn-\hat{O}-Mn \rangle)$. To obtain realistic values of W_a, we have normalized the values from eq 1 by setting the value of the bandwidth to 1 eV when $\langle r_A \rangle$ is ∼1.24 Å. The manganate corresponding to a $\langle r_A \rangle$ value of 1.24 Å is $La_{0.7}Sr_{0.3}MnO_3$. In Figure 11, we show

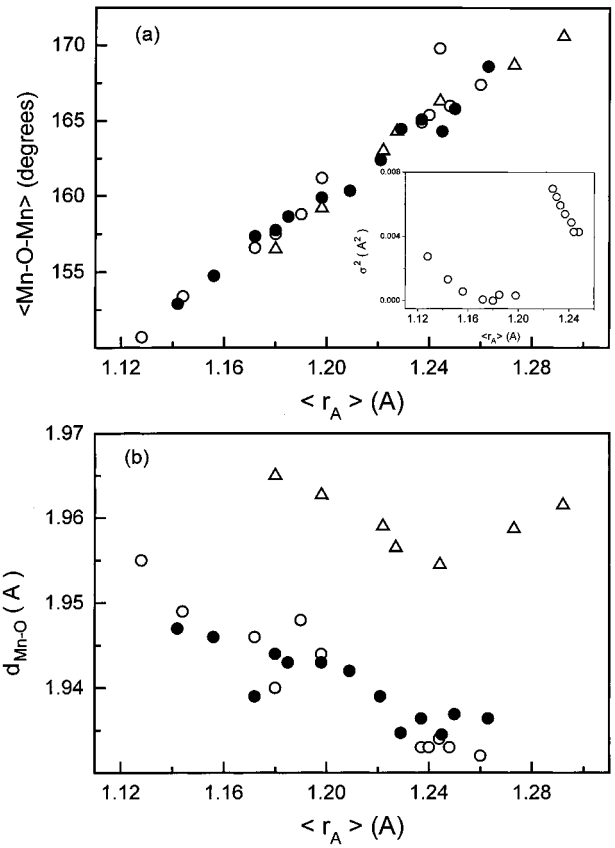

Figure 10. Variation of (a) the Mn−O−Mn angle and (b) the average Mn−O distance with $\langle r_A \rangle$: $Ln_{0.5}A_{0.5}MnO_3$ (circles), and $Ln_{0.7}A_{0.3}MnO_3$ (triangles) for various A ions. Filled circles are recent data from ref 23 on $Ln_{0.5}A_{0.5}MnO_3$. For explanation of inset in panel a, see text at the end of section 3.

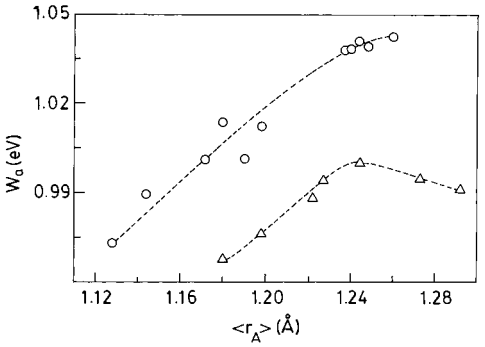

Figure 11. Variation of the apparent bandwidth, W_a, of the manganates with $\langle r_A \rangle$. Notice the small change in W_a over the entire range of $\langle r_A \rangle$ (from Arulraj et al.[20b]).

the variation of W_a with $\langle r_A \rangle$ for both the $Ln_{0.7}A_{0.3}MnO_3$ and $Ln_{0.5}A_{0.5}MnO_3$ compositions. This figure represents the variation of the apparent bandwidth with $\langle r_A \rangle$, based on purely geometrical factors, as defined by eq 1. The apparent bandwidth shows a maximum in the case of $Ln_{0.7}A_{0.3}MnO_3$ at an $\langle r_A \rangle$ value of ∼1.24 Å, with the suggestion of a plateau above this $\langle r_A \rangle$ value in the case of $Ln_{0.5}A_{0.5}MnO_3$. What is noteworthy is that the change in W_a over the entire $\langle r_A \rangle$ range is rather small, although T_{CO} and T_c vary significantly with $\langle r_A \rangle$ (Figure 12). Thus, the variation of the ferromagnetic T_c and of the "real" e_g-level bandwidth W of $Ln_{1-x}A_xMnO_3$ with the average A-site cationic radius $\langle r_A \rangle$ pose a problem. Note, for $\Delta\langle r_A \rangle \cong 1.26 - 1.24$ Å $= 0.02$ Å, we have $\Delta T_c \cong 350 - 250$ K $= 100$ K. Inasmuch as both T_c and W

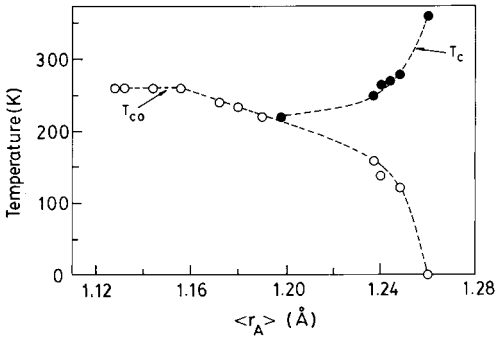

Figure 12. Variation of the charge-ordering transition temperature, T_{CO}, and the ferromagnetic Curie temperature, T_c, of the manganates with $\langle r_A \rangle$.

scale with the orbital overlap of O:2pσ with Mn:3d$_{x^2-y^2}$, which in turn is an increasing function of the Mn−O−Mn bond angle $\Theta(=\pi-\omega)$, and therefore of $\langle r_A \rangle$, we expect T_c and hence the real bandwidth to increase with $\langle r_A \rangle$ more drastically than depicted by Figure 11. The angular variation of the orbital overlap $\sim(1 - \cos \omega/2)$ is too small (=5%) to account for the relatively large observed change of T_c that scales as $(1 - \cos \omega/2)^2$ due to double exchange, or of W that scales as $(1 - \cos \omega/2)$.

The inadequacy of the Mn−O−Mn bond angular variation to explain the changes in T_c with $\langle r_A \rangle$ prompts us to consider covalent mixing effects associated with the changes in $\langle r_A \rangle$. Our reasoning is along the lines employed by Goodenough[25] in the context of $Ca_{1-x}Sr_x$-MnO_3. Goodenough explained the enhancement of T_N in $Ca_{1-x}Sr_xMnO_3$ with increasing x successfully in terms of the lower covalent mixing of the larger A-site cation Sr. The covalent mixing of the A-site cation with the anion O:2pπ would normally compete with that between the anion and the B-site cation Mn:3d-t_{2g}, thus reducing the superexchange coupling. In the case of $Ln_{1-x}A_xMnO_3$ with the electronically mobile Mn^{3+}−O−Mn^{4+} units, in contrast to $Ca_{1-x}Sr_xMnO_3$ with the immobile Mn^{4+}−O−Mn^{4+} units, we can invoke the covalent mixing, but of the anion O:2pσ with the A-site cation as competing against its covalent mixing with the B-site cation Mn:3d-e_g. Thus, with increasing $\langle r_A \rangle$ and, hence, decreasing A-site covalent mixing, we would expect an increasing e_g bandwidth W as well as the double-exchange coupling T_c. This covalent mixing effect is expected to be intrinsically much larger than the geometric (angular) effect (discussed earlier with W_a). Furthermore, the covalent mixing effect on W and T_c (double-exchange) is considerably stronger than on the super exchange (antiferromagnetic T_N), because the latter is of higher (fourth) order in the orbital overlap involved. We note that when $\langle r_A \rangle$ is ~1.24 Å, the Mn−O bond is shorter and more covalent, becoming increasingly ionic as $\langle r_A \rangle$ decreases (Figure 10). When $\langle r_A \rangle < 1.17$ Å, the Mn−O bond is nearly ionic, with the distance closely corresponding to the sum of the ionic radii.

It has been shown that T_c values of the manganates are significantly affected by the A-site cation disorder arising from the mismatch in the sizes of the ions (Ln and alkaline earth).[26] This effect has been rationalized in terms of the variance of the size distribution, σ^2. A proper treatment of the σ^2 effect on charge-ordering in manganates would be possible only if we had the data on several manganates with the same $\langle r_A \rangle$. Unfortunately, we do not have such data. The available data are shown as a $\sigma^2-\langle r_A \rangle$ plot in the inset of Figure 10a. We see that in the region of large T_{CO} or small $\langle r_A \rangle$, the σ^2 is close to zero. Actually, in the $\langle r_A \rangle$ region 1.13−1.17 Å, T_{CO} varies only slightly, but σ^2 increases with a decrease in $\langle r_A \rangle$. The higher σ^2 could decrease T_{CO}; T_{CO} at small $\langle r_A \rangle$ could otherwise be higher. Interestingly, σ^2 is high when T_{CO} is small (Figure 10a). In other words, high σ^2 tends to destroy charge-ordering and renders the manganate ferromagnetic as suggested by Damay et al.[26b]

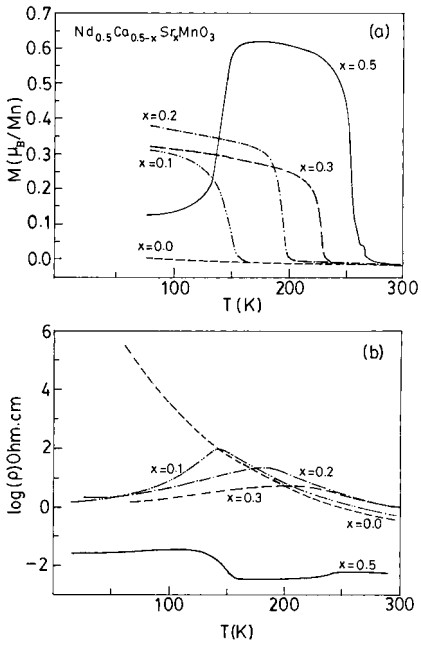

Figure 13. Temperature variation of (a) the magnetization and (b) the resistivity of the $Nd_{0.5}Ca_{0.5-x}Sr_xMnO_3$ compositions (from Rao et al.[29b]).

4. Effect of Internal Pressure

Recall that the ferromagnetic T_c of manganates of composition $La_{0.7}A_{0.3}MnO_3$ exhibiting CMR increases with the average radius of the A-site cations, just as with external pressure.[27] External pressure has been shown to lower the charge-ordering transition temperature in the manganates.[28] A detailed study of the effect of internal pressure on charge-ordering has been carried out by varying $\langle r_A \rangle$ in several manganate systems.[29] In $Pr_{0.7}Ca_{0.3-x}Sr_xMnO_3$ and $Nd_{0.5}Ca_{0.5-x}Sr_xMnO_3$, the material undergoes an insulator−metal transition with increasing x; in the metallic phase, the material is ferromagnetic (Figure 13). Similar effects are seen in $Pr_{0.7-x}La_xCa_{0.3}MnO_3$ as well. Generally, increasing $\langle r_A \rangle$ or the internal pressure decreases T_{CO} and increases T_c. At very high pressures, these materials become ferromagnetic metals in the ground state.[30]

5. Chemical Melting of the Charge-Ordered State

Cation substitution in the Mn site of CO manganates has a profound effect in the electronic and magnetic properties of the materials. Raveau and co-workers[31] reported that substitution of Al^{3+}, Fe^{3+}, Cr^{3+} and other ions often brings about an insulator−metal transition in the otherwise CO insulators. The two types of CO

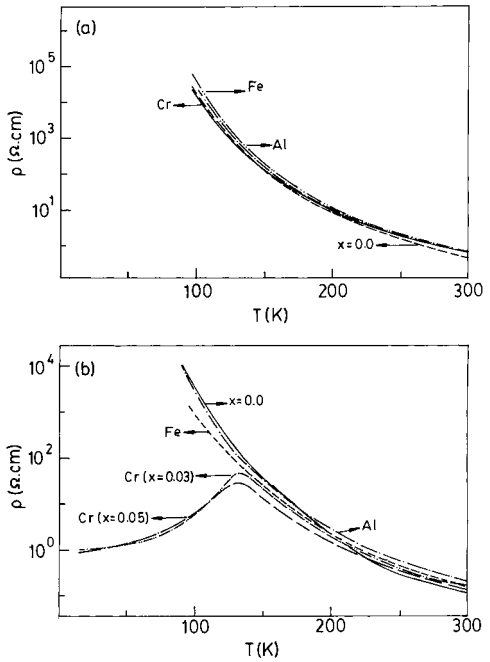

Figure 14. Temperature variation of the resistivity of $Ln_{0.5}Ca_{0.5}Mn_{1-x}M_xO_3$: (a) Ln = Y for different M ($x = 0.03$), (b) Ln = Nd, M = Al, and Fe ($x = 0.03$) and M = Cr ($x = 0.03$ and 0.05) (from Vanitha et al.[32]).

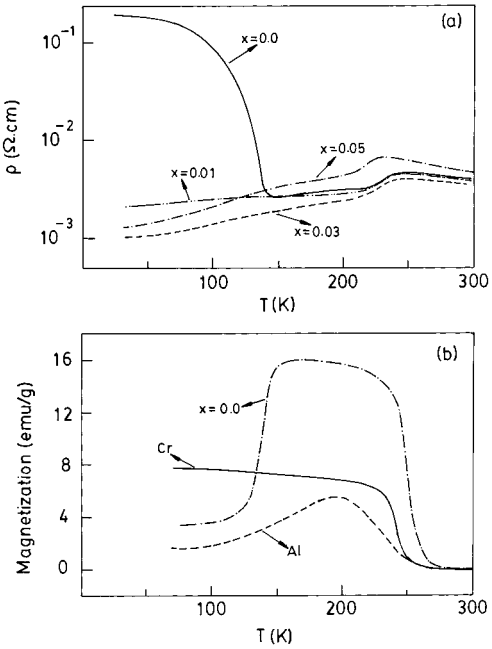

Figure 15. Temperature variation of (a) the resistivity of $Nd_{0.5}Sr_{0.5}Mn_{1-x}Cr_xO_3$ and (b) the magnetization of $Nd_{0.5}Sr_{0.5}Mn_{1-x}M_xO_3$ (M = Cr, Al, $x = 0.03$) (from Vanitha et al.[32]).

states in the manganates can be delineated through B-site substitution.[32] The insulating CO state of $Ln_{0.5}Ca_{0.5}MnO_3$ (Ln = Nd, Gd, or Y) is unaffected by substitution with Al^{3+} and Fe^{3+}, but the CO state in the Nd compound ($\langle r_A \rangle = 1.17$ Å) is melted into a FMM state by Cr^{3+} substitution (Figure 14). Progressive substitution of Mn^{3+} in $Nd_{0.5}Sr_{0.5}MnO_3$ ($\langle r_A \rangle = 1.24$ Å) by Al^{3+} or Fe^{3+} renders it an insulator. Substitution with Cr^{3+}, however, makes it a ferromagnetic metal from 250 K down to low temperatures, without the intervening CO state as in the parent material (Figure 15). The role of Cr^{3+} in melting the CO state is not clear at present.

6. Other Effects

Application of an electric field appears to collapse the CO state in $Pr_{0.7}Ca_{0.3}MnO_3$.[33] X-ray irradiation of $Pr_{0.7}Ca_{0.3}MnO_3$ brings about a transition of the CO insulating state to a FMM state.[34] Recent measurements on the epitaxial films of $Nd_{0.5}Ca_{0.5}MnO_3$ carried out in Bangalore show that small dc voltages of 1−10 V bring about the insulator−metal transition. There are interesting hysteresis effects in the resistivity−voltage plots, suggesting applications. X-ray irradiation at low temperature seems to create ferromagnetic clusters, which grow to melt the CO state at high exposures.[35] Photocarrier injection with of a YAG laser also induces an insulator−metal transition in $Pr_{0.7}Ca_{0.3}MnO_3$.[36]

7. Complex Transitions

We mentioned earlier that the manganates in region C of the phase diagram in Figure 8 (or regions III and IV in Figure 9) may exhibit complex magnetic and electronic properties. We illustrate this aspect by two careful investigations reported recently. Charge-ordering has been investigated in $(Nd_{1-x}Sm_x)_{0.5}Sr_{0.5}MnO_3$ ($0 = x = 1$) by varying $\langle r_A \rangle$ or by applying external pressure.[37] Competition between double-exchange (FM) and charge-ordering (AFM) interactions give rise to complex metal−insulator phase diagrams with temperature, pressure, or x as the parameter. A pressure-induced transition from a FM to a stable CO insulator has been found for $x = 0.875$. With a decrease in $\langle r_A \rangle$, the CO instability persists even above the ferromagnetic T_c and enhances the electron−lattice coupling. Accordingly, a lattice-coupled first-order insulator−metal transition occurs at T_c when $x = 0.5$. In the analogous manganate, $Nd_{0.25}La_{0.25}Ca_{0.5}MnO_3$, a reentrant transition from an incipient CO state to a FMM state has been established.[38] The reentrant phase is associated with a first-order phase transition that reduces the orthorhombic distortion in the lattice, in contrast to the CO transition in other manganates where the orthorhombic distortion increases at low temperatures. At the CO−FMM transition, a collapse in the charge-ordering gap has been observed directly by vacuum tunneling spectroscopy (Figure 16). The J−T distortion of the MnO_6 octahedra becomes maximum before the reentrant transition, accompanying the sharp decrease in resistivity and the collapse of the CO gap. It is noteworthy that in the $(Nd_{1-x}Sm_x)_{0.5}Sr_{0.5}$ system, the variance due to ion size mismatch, σ^2, increases with increase in x (see inset of Figure 10a) and this would explain some of the observed properties. Similarly, in the $Nd_{0.25}La_{0.25}Ca_{0.5}$ compound we would also expect a lower T_{CO} and ferromagnetism due to the higher σ^2.

The phase transitions in $Nd_{0.5}Sr_{0.5}MnO_3$ have been studied carefully by synchrotron X-ray diffraction.[39] The study shows that the FMM state, the CO state, and probably the orbitally ordered state coexist around 150 K, which has been believed to be the T_{CO}. Thus, a transition to an intermediate (orbitally ordered) phase from the FMM state starts at ~200 K, well before T_{CO}. At low temperatures ($T \ll T_{CO}$), a small fraction of the

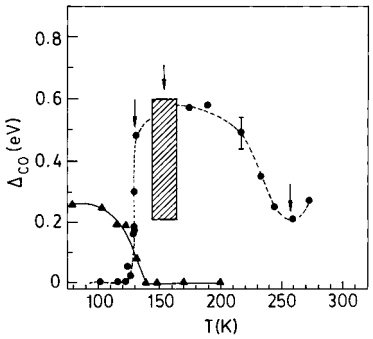

Figure 16. Temperature variation of the charge-ordering gap, Δ_{CO}, in $Nd_{0.5}Sr_{0.5}MnO_3$ (triangles) and in $Nd_{0.25}La_{0.25}Ca_{0.5}MnO_3$ (circles) (from Arulraj et al.[38]). Shaded region corresponds to the first-order transition.

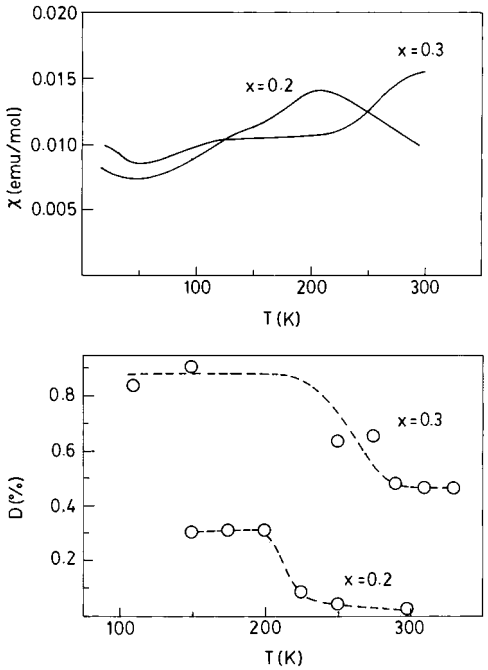

Figure 17. Temperature variation of (a) magnetic susceptibility and (b) the lattice distortion index in $Bi_xCa_{1-x}MnO_3$ (from Arulraj et al.[43]).

FMM state persists along with the CO and orbitally ordered phases. Such a coexistence of phases in $Nd_{0.5}Sr_{0.5}MnO_3$ makes the CO manganates truly interesting systems to investigate further with respect to the phase stabilities and transitions. This apparent contradiction of the phase rule needs to be explained by considering the different identities of the three phases of the same stoichiometry.

8. Other Manganates

Charge-ordering in the quasi-two-dimensional $Ln_{0.5}Sr_{1.5}MnO_4$ occurs at 230 K when Ln = La, but disappears when Ln = Nd.[40] In layered $LaSr_2Mn_2O_7$, an additional superstructure in the electron diffraction pattern found at low temperatures has been interpreted as due to charge-ordering associated with the d_{z^2} orbital ordering of Mn^{3+}.[41]

A study of $Bi_xCa_{1-x}MnO_3$ ($0.74 = x = 0.82$) has shown that the nature of spin fluctuations changes from ferromagnetic to antiferromagnetic at the charge-ordering transition (~210 K).[42] There is a structural transition around T_{CO}, and an antiferromagnetic transition occurs at still lower temperatures. In Figure 17a, we show the temperature variation of the magnetic susceptibility of two compositions of $Bi_xCa_{1-x}MnO_3$.[43] We notice that T_{CO} in the $x = 0.3$ composition is above 300 K; there is a susceptibility anomaly at ~130 K due to T_N. The T_{CO} decreases to 210 K when $x = 0.2$, but the T_N remains unaffected. At the T_{CO}, the activation energy for conduction shows a maximum and the structure changes from pseudocubic to O′-orthorhombic. The lattice distortion index, D, increases from 0.4 to 0.9% at T_{CO} in the $x = 0.3$ composition (Figure 17b). When $T > T_{CO}$, ferromagnetic double-exchange interaction promotes the hopping of J−T polarons. The high sensitivity of T_{CO} in $Bi_xCa_{1-x}MnO_3$ to composition is noteworthy, although $\langle r_A \rangle$ is hardly affected, suggesting the role of $Mn^{3+}-O-Mn^{4+}$ interaction in determining the value of T_{CO}. These results also lend credence to the explanation based on the competition between Mn (σ) and O (σ) and A (σ)−O (σ) bonding.

Charge-ordering occurs in nonstoichiometric $CaMnO_{3-\delta}$, particularly for $\delta = 0.18$, which corresponds to $x = 4/5$ doping. The magnetic susceptibility shows a transition starting at 250 K. Around this temperature, the resistivity also shows an anomalous increase.

9. Concluding Remarks

The short account of charge-ordering in the manganates should clearly show how this phenomenon gives rise to a wide variety of fascinating electronic and magnetic properties that are subtly controlled by the cation size and related factors. There are very few metal oxide systems where such fabulous changes in properties (e.g., metallic, insulating, magnetic, structural) occur accompanying such minor changes in composition. Furthermore, the sensitivity of the CO state to magnetic and electric fields, laser irradiation, and chemical substitution suggests many possible applications, besides providing a rich area for research. Many other manganates, such as the layered ones, need to be investigated in greater detail. The complex regime in the phase diagram where novel magnetic and electronic properties manifest themselves because of competing interactions deserves greater attention. Clearly, charge-ordering in the manganates is unique because Mn^{3+} is a J−T ion and the $Mn^{3+}-O-Mn^{4+}$ units promote double-exchange. The complexity of the phase transitions in $Nd_{0.5}Sr_{0.5}MnO_3$, in apparent contradiction of the phase rule, is truly interesting and requires further study. There is considerable scope for theoretical and computer simulation studies of the different types of CO states. There has been some effort to examine charge-ordering in $Ln_{0.5}A_{0.5}MnO_3$ based on a Hamiltonian of small polarons with strong nearest-neighbor repulsion[44] and in terms of an interplay between double-exchange, superexchange, and coulomb interaction terms in the Hamiltonian.[45] Spin-ordered and CO states with domain walls in 2- and 3-dimensional perovskite oxides have also been examined in terms of super exchange interaction.[46] These efforts only mark a beginning.

Acknowledgment. The authors thank Unilever plc for support of a joint research program between JNCASR and UCSB-MRL.

References

(1) Honig, J. M. In *The Metallic and the Nonmetallic States of Matter*; Rao, C. N. R., Edwards P. P., Eds.; Taylor and Francis: London, 1985.
(2) Berry, F. J.; Skinner, S.; Thomas, M. F. *J. Phys.: Condens. Matter* **1998**, *10*, 215.
(3) Samiulla, M. *Phys. Rev.* **1995**, *B51*, 10352.
(4) Li, J. Q.; Matsui, Y.; Park, S. K.; Tokura Y. *Phys. Rev. Lett.* **1997**, *79*, 297.
(5) Blumberg, G.; Klein, M. V.; Cheong, S. W. *Phys. Rev. Lett.* **1998**, *80*, 564. (b) Katsufuji, T.; Tanabe, T.; Ishikawa, T.; Fukuda, Y.; Arima, T.; Tokura, Y. *Phys. Rev.* **1996**, *B54*, 14230.
(6) Wollan, E. O.; Koehler, W. C. *Phys. Rev.* **1955**, *100*, 545. (b) Jirak, Z.; Krupicka, S.; Simsa, Z.; Dlouha, M.; Vratislav, S. *J. Magn. Magn. Mater.* **1985**, *53*, 153.
(7) Rao, C. N. R.; Cheetham, A. K.; Mahesh, R. *Chem. Mater.* **1996**, *8*, 2421. (b) Rao, C. N. R.; Cheetham, A. K. *Adv. Mater.* **1997**, *9*, 1009 and the references therein.
(8) Kuwahara, H.; Tomioka, Y.; Asamitsu, A.; Moritomo, Y.; Tokura, Y.; *Science* **1995**, *270*, 961.
(9) Laffez, P.; Van Tendeloo, G.; Millange, F.; Caignaert, V.; Raveau, B. *Mater. Res. Bull.* **1996**, *31*, 905.
(10) Biswas, A.; Raychaudhuri, A. K.; Mahendiran, R.; Guha, A.; Mahesh, R.; Rao, C. N. R. *J. Phys. Condens. Matter* **1997**, *9*, L355.
(11) Kawano, H.; Kajimoto, R.; Yoshizawa, H.; Tomioka, Y.; Kuwahara, H.; Tokura, Y. *Phys. Rev. Lett.* **1997**, *78*, 4253.
(12) Tomioka, Y.; Asamitsu, A.; Kuwahara, H.; Moritomo, Y.; Tokura, Y. *Phys. Rev.* **1996**, *B53*, 1689. (b) Tokunaga, M.; Miura, N.; Tomioka, Y.; Tokura, Y. *Phys. Rev.* **1998**, *B57*, 5259.
(13) Vogt, T.; Cheetham, A. K.; Mahendiran, R.; Raychaudhuri, A. K.; Mahesh, R.; Rao, C. N. R. *Phys. Rev.* **1996**, *B54*, 15303.
(14) Yoshizawa, H.; Kawano, H.; Tomioka, Y.; Tokura, Y. *Phys. Rev.* **1995**, *B52*, 13145.
(15) Tokura, Y.; Tomioka, Y.; Asamitsu, A.; Moritomo, Y.; Kasai, M. *J. Appl. Phys.* **1996**, *79*, 5288.
(16) Ramirez, A. P.; Schiffer, P.; Cheong, S. W.; Chen, C. H.; Bao, W.; Palstra, T. T. M.; Gammel, P. L.; Bishop, D. J.; Zegarski, B. *Phys. Rev. Lett.* **1996**, *76*, 3188. (b) Ibarra, M. R.; De Teresa, J. M.; Blasco, J.; Algarabel, P. A.; Marquina, C.; Garcia, J.; Stankiewiez, J.; Ritter, C. *Phys. Rev.* **1997**, *B56*, 8252.
(17) Radaelli, P. G.; Cox, D. E.; Marezio, M.; Cheong, S. W. *Phys. Rev.* **1997**, *B55*, 3015.
(18) Chen, C. H.; Cheong, S. W.; Hwang, H. Y. *J. Appl. Phys.* **1997**, *81*, 4326.
(19) Mori, S., Chen, C. H., Cheong, S. W. *Nature* **1998**, *392*, 473.
(20) Arulraj, A.; Gundakaram, R.; Biswas, A.; Gayathri, N.; Raychaudhuri, A. K.; Rao, C. N. R. *J. Phys. Condens. Matter* **1998**, *10*, 4447. (b) Arulraj, A.; Santosh, P. N.; Gopalan, R. S.; Guha, A.; Raychaudhuri, A. K.; Kumar, N.; Rao, C. N. R. *J. Phys. Condens. Matter* **1998**, *10*, 8497.
(21) Kumar, N.; Rao, C. N. R. *J. Solid State Chem.* **1997**, *129*, 363.
(22) Radaelli, P. G.; Iannone, G.; Marezio, M.; Hwang, H. Y.; Cheong, S. W.; Jorgensen, J. D. Argyriou, D. N. *Phys. Rev.* **1997**, *B56*, 8265.
(23) Woodward, P. M.; Vogt, T.; Cox, D. E.; Arulraj, A.; Rao, C. N. R.; Karen, P.; Cheetham, A. K. *Chem. Mater.*, in press.
(24) Medarde, M.; Mesot, J.; Lacorre, P.; Rosenkranz, S.; Fischer, P.; Gobrecht, K. *Phys. Rev.* **1995**, *B52*, 9248.
(25) Goodenough, J. B. *Phys. Rev.* **1967**, *164*, 785.
(26) Rodriguez-Martinez, L. M.; Attfield, J. M. *Phys. Rev.* **1996**, *B54*, R15622. (b) Damay, P.; Martin, C.; Maignan, A.; Raveau, B. *J. Appl. Phys.* **1997**, *82*, 6181.
(27) Mahesh, R.; Mahendiran, R.; Raychaudhuri, A. K.; Rao, C. N. R. *J. Solid State Chem.* **1995**, *120*, 204.
(28) Moritomo, Y.; Kuwahara, H.; Tomioka, Y.; Tokura, Y. *Phys. Rev.* **1997**, *B55*, 7549.
(29) Raveau, B.; Maignan, A.; Caignaert, V. *J. Solid State Chem.* **1995**, *117*, 424. (b) Rao, C. N. R.; Santosh, P. N.; Singh, R. S.; Arulraj, A. *J. Solid State Chem.* **1998**, *135*, 169.
(30) Yoshizawa, H.; Kajimoto, R.; Kawano, H.; Tomioka, Y.; Tokura, Y. *Phys. Rev.* **1997**, *B55*, 2729.
(31) Raveau, B.; Maignan, A.; Martin, C. *J. Solid State Chem.* **1997**, *130*, *162*. (b) Barnabe, A.; Maignan, A..; Hervieu, M.; Damay, F.; Martin, C.: Raveau, B. *Appl. Phys. Lett.* **1997**, *71*, 3907.
(32) Vanitha, P. V.; Singh, R. S.; Natarajan, S.; Rao, C. N. R. *J. Solid State Chem.* **1998**, *137*, 365.
(33) Asamitsu, A.; Tomioka, Y.; Kuwahara, H.; Tokura, Y. *Nature* **1997**, *388*, 50.
(34) Kiriyukhin, V.; Casa, D.; Hill, J. P.; Keimer, B.; Vigilante, A.; Tomioka, Y.; Tokura, Y. *Nature* **1997**, *386*, 813.
(35) Cox, D. E.; Radaelli, P. G.; Marezio, M.; Cheong, S. W. *Phys. Rev.* **1998**, *B57*, 3305.
(36) Miyano, K.; Tanaka, T.; Tomioka, Y.; Tokura, Y. *Phys. Rev. Lett.* **1997**, *78*, 4257.
(37) Kuwahara, H.; Moritomo, Y.; Tomioka, Y.; Asamitsu, A.; Kasai, M.; Kumai, R.; Tokura, Y. *Phys. Rev.* **1997**, *B56*, 9386.
(38) Arulraj, A.; Biswas, A.; Raychaudhuri, A. K.; Rao, C. N. R.; Woodward, P. M.; Vogt, T.; Cox, D. E.; Cheetham, A. K. *Phys. Rev.* **1998**, *B57*, R8115.
(39) Woodward, P. M.; Vogt, T.; Cox, D. E.; Rao, C. N. R.; Cheetham, A. K. *Phys. Rev. B*, in press.
(40) Moritomo, Y.; Nakamura, A.; Mori, S.; Yamamoto, N.; Ohoyama, K.; Dhashi, M. *Phys. Rev.* **1997**, *B56*, 14879.
(41) Li, J. Q.; Matsui, Y.; Kimura, T.; Tokura, Y. *Phys. Rev.* **1998**, *B57*, 3205.
(42) Bao, W.; Axe, J. D.; Chen, C. H.; Cheong, S. W. *Phys. Rev. Lett.* **1997**, *78*, 543.
(43) Arulraj, A.; Santhosh, P. N.; Rao, C. N. R., unpublished results.
(44) Lee, J. D.; Min, B. I. *Phys. Rev.* **1997**, *B55*, 14713.
(45) Mishra, S. K.; Pandit, R.; Satpathy, S. *Phys. Rev.* **1997**, *B56*, 2316.
(46) Mizokawa, T.; Fujimori, A. *Phys. Rev. Lett.* **1998**, *80*, 1320.

CM980318E